

A numerical approach to estimate shaft friction of bored piles in sands

Ylenia Mascarucci · Salvatore Miliziano ·
Alessandro Mandolini

Received: 10 August 2013 / Accepted: 14 January 2014 / Published online: 2 February 2014
© Springer-Verlag Berlin Heidelberg 2014

Abstract A new approach to estimate shaft capacity of bored piles in sandy soils, based on numerical analysis, is presented. The topic is relevant as current design methods often largely underestimate the shaft capacity of piles in sands, thus resulting in an over-conservative design. The proposed approach is based on explicitly modelling the thin cylinder of soil surrounding the pile, where strain localization concentrates (shear band), and on the fundamental mechanic behaviour of sandy soils (e.g. dilatancy, softening). This approach is both simple and easy to apply. Results of a broad parametric study involving axially loaded single piles embedded in different sandy soils are presented, highlighting that relative density and grain size distribution mainly affect the shaft capacity. The capability of the procedure to predict shaft friction is checked against data from a well-documented full-scale axial load test on instrumented pile. Some suggestions for calibration and application of the method are also reported.

Keywords Bored piles · Dilatancy · Sand · Shaft friction · Shear band · Soil grading

Y. Mascarucci (✉) · A. Mandolini
Department of Civil Engineering, Design, Building and Environment, Second University of Napoli, Via Roma 29, 81031 Aversa, CE, Italy
e-mail: ylenia.mascarucci@unina2.it

A. Mandolini
e-mail: alessandro.mandolini@unina2.it

S. Miliziano
Department of Structural and Geotechnical Engineering, Sapienza University of Roma, Via Eudossiana 18, 00184 Rome, Italy
e-mail: salvatore.miliziano@uniroma1.it

1 Introduction

Significant advances have been made in identifying processes that occur in the soil zone immediately adjacent to the pile during loading phase. Nevertheless, design methods for bored piles currently used in practice do not explicitly take into account the fundamental aspects of soil behaviour (i.e. void ratio and state of stress). This particularly applies to sandy soils, for which the well-known difficulties in retrieving undisturbed samples have led to a widespread use of in situ test-based methods (often referred to as *empiric* or *direct methods*). The available methods often result in very large scattered predictions, clearly highlighted by so-called prediction events (e.g. [45]). This reinforces the belief that predictive reliability is generally far poorer than many practitioners recognize [17].

The need for a calculation methodology that can yield accurate results is relevant as current design methods often largely underestimate the shaft capacity of piles in sands, thus resulting in an over-conservative and more expensive design. These methods are very simple to apply, but are too simplistic as they do not properly take into account the fundamental aspects of the behaviour of sandy soil nor the complex phenomena occurring in the thin cylinder of soil surrounding the pile, where strain localization occurs (shear band). Consequently, their ability to predict pile behaviour is quite poor.

An attempt to overcome this lack is made here, with particular reference to the shaft capacity of bored cast in situ piles embedded in sands. Based on numerical modelling, the approach presented is relatively practical and simple to be used routinely and, at the same time, it can take into account the main factors on which the phenomena depend. The shear band, which forms close to the shaft during axial loading, is explicitly considered by means of

interface elements, whose constitutive law has been conveniently selected to reproduce the main aspects of the mechanical behaviour of sands.

A brief summary regarding some of the most common methods currently used for the evaluation of pile shaft friction is given. The main aspects of the interaction mechanisms between pile and surrounding soil are then illustrated, and the role played by the dilative behaviour of sand in the shear band, partially restrained by the surrounding soil, is highlighted.

Numerical analyses performed by means of FLAC 2D are focused on. Following the description of the numerical modelling procedure, results obtained for an axially loaded single pile are presented in some detail. The results of a broad parametric study are then discussed, with the aim of detecting which parameters play a major role on shaft friction (relative density, geostatic stresses, strength and shear band thickness, etc.).

The predictive capability of the proposed approach is checked against a selected full-scale axial load test on instrumented pile [5, 46].

2 Background

The evaluation of the ultimate shaft friction, q_s , at a given depth, z , along a vertical pile embedded into a sandy soil, is usually made by methods based on soil properties (so-called *theoretical methods*) or directly on in situ test results (so-called *empirical methods*). For both approaches, several indications are given in Recommendations, Guides or Codes; a detailed overview is currently available in many textbooks (e.g. [13, 48]).

Regarding theoretical methods, the starting point for estimating values of shaft friction q_s for a vertical pile in sandy soil is the expression:

$$q_s = \sigma'_{hr} \cdot \tan \delta' = K \cdot \sigma'_{v0} \cdot \tan \delta' = \beta \cdot \sigma'_{v0} \tag{1}$$

where σ'_{hr} is the effective horizontal stress at failure and δ' represents the soil–pile friction angle. The normal effective stress may be taken as some ratio K of the vertical effective stress σ'_{v0} , thus resulting in the second form of the expression in Eq. 1. Usually, the appropriate value of K depends on (1) the in situ earth pressure coefficient, K_0 , (2) the method of installation of the pile and (3) the initial relative density of the sand, I_D .

Instead of separately evaluating K and $\tan \delta'$, in routine design practice it is often suggested to refer to a lumped parameter, $\beta = K \cdot \tan \delta'$ [30], giving rise to the well-known β methods (third form of the expression in Eq. 1). The original β method for piles embedded in granular soils, first introduced by Reese and O’Neill [37] on the basis of 41 load tests on bored piles, typically underestimates shaft

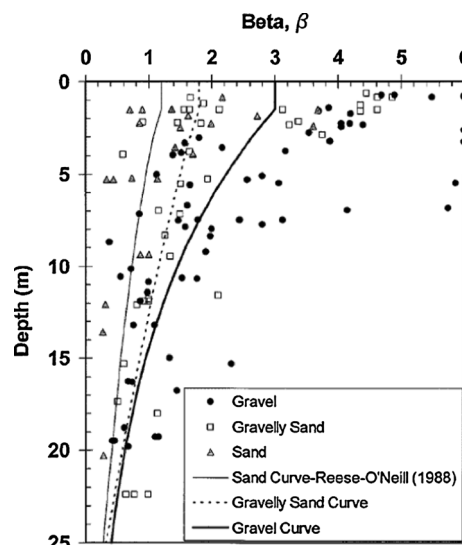


Fig. 1 Experimental β values from load tests of bored piles in fine and coarse sands, compared with Reese and O’Neill [37] and Rollins et al. [38] design curves (modified from [38])

resistance since it was developed as the lower bound of experimental data. The conservatism of such an approach was demonstrated by Rollins et al. [38] (Fig. 1), who back-figured more than one hundred tensile load tests on bored piles in sands and gravels and suggested different depth-depending β curves.

Irrespective of the specific suggestions given by Rollins et al. [38], data in Fig. 1 show that (1) β decreases for increasing depth and (2) at a given depth larger values for β are expected passing from sand to gravel.

Recently, FHWA [11] proposed the so-called *rational β method* for bored cast in situ piles, where the coefficient K is set equal to the earth coefficient at rest K_0 (hence $\beta = \beta_0 = K_0 \cdot \tan \delta'$). The latter can be evaluated by the expression of Mayne and Kulhawy [28]:

$$K_{0,OC} = K_{0,NC} \cdot OCR^{\sin \phi'} \tag{2}$$

where OCR is the over-consolidation ratio, $K_{0,NC} = 1 - \sin \phi'$ following Jaky [15] and ϕ' is the friction angle of the soil; at shallow depth ($z \leq 2.3$ m), a constant value $K = K_{0,OC}$ (calculated at $z = 2.3$ m) is suggested. The soil–pile interface friction angle δ' is assumed to be coincident with ϕ' .

Figure 2 reports the comparison between β values suggested by FHWA [11] and those experimentally measured by more than 100 load tests on piles [7]. When normally consolidated soils (NC, OCR = 1) are assumed, typical values for ϕ' lead to β in the range 0.25–0.30, hence largely underestimating experimental data. To obtain higher values of β , very large ϕ' and OCR have to be considered. In Fig. 2, the curve “OC” refers to over-consolidated soils, having $\phi' = 45^\circ$ and OCR decreasing with depth, from

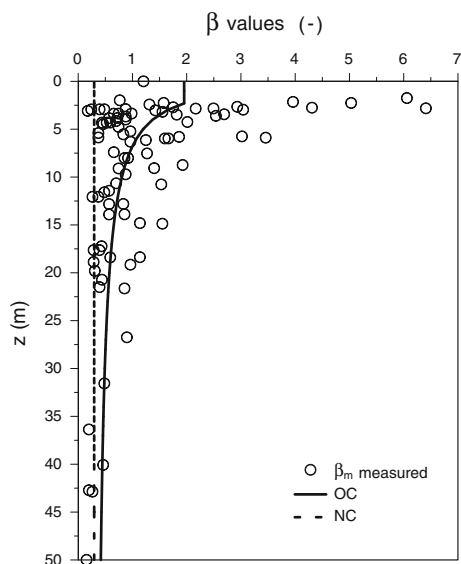


Fig. 2 Experimental mean β_m values from axial load tests of bored piles in sand [7], compared with β_0 values for NC and OC soils (modified from [11])

more than 30 close to the ground surface to about 2 at $z = 40$ m, thus corresponding to very large K_0 values ranging between over 3 to about 0.4. It should be noted that several measures are still larger than the predicted values. Moreover, this approach yields results in terms of K_0 , which are in evident contrast with some experimental data: Jamiolkowski et al. [16], on the basis of calibration chamber tests results, found that also in heavily OC sandy soils ($OCR_{max} = 15$) $K_{0,OC}$ is not greater than 1.

Therefore, it clearly follows that the estimation of q_s in Eq. 1 is challenging.

Pile installation and loading are a process that causes complex stress changes in the soil around the pile from the in situ conditions to failure. According to Randolph and Gourvenec [34], “a design method is more robust if it has some basis in the underlying mechanics of the process (rather than being wholly empirical)”.

Concerning the aforementioned, complexities arise from the need to estimate the net result of installation and loading effects, based merely on knowledge of the in situ conditions prior to pile installation, as identified by geotechnical site and laboratory investigations.

To tackle the problem, it is useful to separate single contributions to shaft resistance, rewriting Eq. 1 as:

$$q_s = \sigma'_{hf} \cdot \tan \delta' = (\sigma'_{h0} + \Delta\sigma'_{hc} + \Delta\sigma'_{hl}) \cdot \tan \delta' \quad (3)$$

where $\Delta\sigma'_{hc}$ and $\Delta\sigma'_{hl}$ represent the stress changes induced by pile installation and loading, respectively.

The stress change $\Delta\sigma'_{hc}$ depends on the drilling operation (e.g. with or without casing or mud), as well as on the concrete casting and properties (e.g. water/cement ratio).

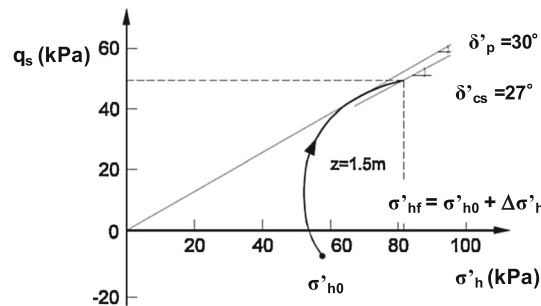


Fig. 3 Typical measured q_s versus σ'_h acting on pile shaft during loading (modified from [19])

According to Fleming et al. [13], if excavation is properly executed and high fluidity concrete is then placed, it is reasonable to assume $\Delta\sigma'_{hc} = 0$, implying that concreting can reinstate the effective horizontal stresses existing before drilling. It is worth noting that, even under this circumstance, the ensuing concrete curing could alter the state of stress in the soil [10, 26].

The stress change $\Delta\sigma'_{hl}$ can be attributed to Poisson’s ratio strains in the pile and to dilation of the soil close to the pile where strains localize, both causing outward expansion towards the surrounding soil for piles under compressive load.

With reference to Poisson’s effect, De Nicola and Randolph [9] carried out a number of numerical analyses and showed that this depends on different parameters (pile geometry, soil and pile properties). Overall, for compressive axial loading, a stress increase of about 10–30 % along the entire pile length can be expected.

Recent research has led to an improved understanding of effects of soil dilation.

Pile response to axial loading is mainly governed by the behaviour of a thin cylinder of soil (shear band) surrounding the pile itself. Lehane et al. [19] highlighted that the increase, u_r , of the thickness, t_s , of such a shear band induced by soil dilatancy, determines an increase of the effective horizontal stress acting on the pile shaft at failure (Fig. 3), as this is partially restrained by the outer soil.

A first attempt to quantify $\Delta\sigma'_{hl}$ was made by Wernick [49]. Starting from an initial state (Fig. 4a), when the soil adjacent to the pile shaft dilates of a quantity u_r the outer soil, schematically represented by springs with a stiffness k_1 , reacts with stresses depending on the geometry of the problem and on soil properties (Fig. 4b). If the theory of expansion of the cylindrical cavity in a linear elastic medium is considered [4]:

$$\Delta\sigma'_{hl} = \frac{4 \cdot G}{D} \cdot u_r = k_1 \cdot u_r \quad (4)$$

where G is the soil shear modulus and D is the pile diameter. The term $k_1 = 4 \cdot G/D$ represents the confining

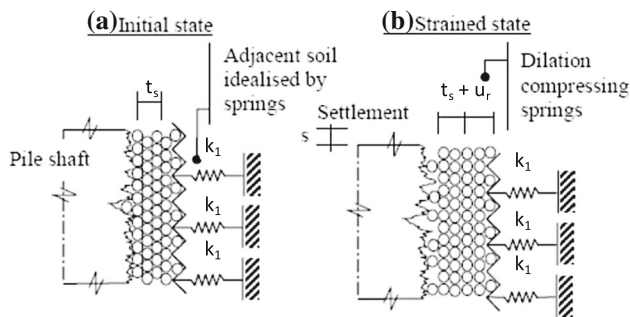


Fig. 4 Wernick [49] model: restraining effect on shear band dilation (modified from [49])

stiffness imposed by the surrounding soil, which decreases for increasing pile diameter.

From Eq. 4, it clearly derives that a reliable estimate of $\Delta\sigma'_{hl}$ strictly depends on the assessment of G and u_r .

To take into account the nonlinearity of soil behaviour, the use of linear elasticity theory requires operative values for G to be selected. For instance, Fioravante [12] suggests $G = (0.05\text{--}0.10) \cdot G_0$, G_0 being the small strain shear modulus.

The outward displacement is typically evaluated by relating it to the pile roughness, R_a , and/or to the mean particle grain size, D_{50} ($R_a = R_t/2$, where R_t is the vertical distance between the highest peak and the lowest trough measured on a reference length of surface profile, which depends on D_{50} [44]). For instance, Schneider [42] suggests $u_r = 2.5 \cdot D_{50}^{0.4} \cdot R_a^{0.6}$, while Lehane et al. [19] report $u_r = 0.7 \cdot D_{50}$. It is evident that these suggestions do not explicitly take into account the fundamental mechanical behaviour of sandy soil and, in particular, the dependence of soil dilation/contraction on the relative density, I_D , and the mean effective confining stress, p' (e.g. [1]).

Improvements have been provided by Lehane et al. [20], who derived an analytical relationship between dilation and the stiffness of the soil surrounding the shear band. Such an expression has only been calibrated against centrifuge tests and its use requires (1) constant normal load interface shear tests and (2) the stiffness k_1 under cavity expansion of the sand mass surrounding the pile. Based on distinct element numerical modelling of mono-granular sand, Peng et al. [33] recently suggested a similar expression.

Loukidis and Salgado [22] carried out broad parametric finite element numerical analyses using an advanced constitutive model [24] capable of considering the role played by a number of factors affecting q_s (K_0 , σ'_{v0} , I_D and shear band thickness). The results were summarized in an analytical expression for directly estimating $\Delta\sigma'_{hl}$ for pile embedded in clean sand, although some criticism can be made.

From the above, it can be concluded that although the basic mechanisms of pile–soil interaction are quite clear, a

design methodology based on the mechanical behaviour of sandy soils and, at the same time, simple to use in practice, is not yet available.

3 Numerical modelling

Numerical modelling of shaft friction of a bored pile should reproduce the main phenomena that occur at pile–soil contact. Which constitutive law to choose for the soil and which strategies to deal with shear band modelling are rather crucial.

Among the several constitutive models available for the soil, in the authors' opinion the final choice should be that of selecting a model able to combine simplicity and completeness (the former aimed to be effective for practical purposes, the latter aimed to simulate, as best as possible, the shear strain evolution at the pile shaft). In particular, it should be able to describe (1) nonlinear soil behaviour, from small to large strains, (2) soil softening and evolution of plastic strains and (3) the achievement of critical state conditions at large strains.

When dealing with a boundary value problem in the Cauchy continuum, at collapse it is well known that the solutions obtained through numerical methods, such as finite different or finite element, are mesh dependent. However, in the case of pile–soil contact, since the exact location of shear band is known a priori (parallel and adjacent to sand–concrete contact), appropriate results can be obtained by modelling the shear band using continuum elements close to the pile, whose width is set to be equal to the real shear band thickness (e.g. [22]). Alternatively, the shear band can be simulated by means of interface elements, thus shear band behaviour is described in terms of relative displacements between soil and pile, rather than strains (e.g. [3]).

3.1 Soil constitutive model

The strain softening constitutive model (SS) was adopted since it can reproduce the essential features of soil behaviour as, for instance, shown in Fig. 5 for a constant normal load (CNL) simple shear test. It is a relatively simple linear elasto-plastic model with Mohr–Coulomb failure criterion and a non-associated flow rule. The response is initially linear elastic; after yielding, isotropic soil softening is assumed, regulated by plastic shear strains [50].

For a cohesion-less soil (like sand typically is), if it is assumed that both angles of friction, ϕ' , and dilation, ψ , linearly reduce with plastic shear strains from peak to critical state (CS) condition (Fig. 5b), only six parameters (physically based and obtainable by routine geotechnical

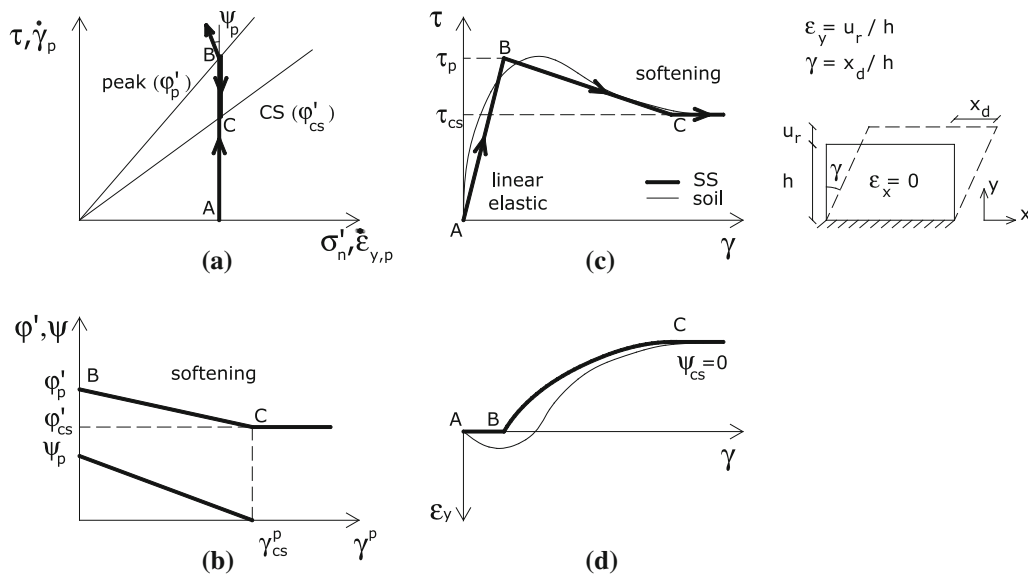


Fig. 5 SS prediction and soil response for CNL simple shear test: **a** stress path; evolution of **c** shear stresses and **d** vertical strains; **b** linear reduction for angle of friction and dilation

Table 1 SS parameters

Shear modulus	G
Poisson's ratio	ν'
Angle of friction at peak condition	ϕ'_p
Angle of friction at critical state condition	ϕ'_{cs}
Angle of dilation at peak condition	ψ_p
Plastic shear strains to get CS condition	γ^p_{cs}

tests) are needed (Table 1): shear modulus, G ; Poisson's ratio, ν' ; friction angle at peak and at CS conditions, ϕ'_p and ϕ'_{cs} , respectively; angle of dilation at peak, ψ_p ; plastic shear strain to achieve CS condition, γ^p_{cs} .

Apart from the nonlinear experimental behaviour observed before the peak, the SS model can be calibrated to better reproduce peak and CS strength as well as the volumetric expansion due to dilatancy. In other words, despite elastic linearity, the model can account for the overall nonlinear behaviour of soil by means of the Mohr–Coulomb failure criterion, whose position in the effective stress space changes according to shear plastic strains (softening).

It is worth noting that the SS model does not include voids ratio but rather its derivatives, such as the tendency to dilate and contract. In detail, the volumetric plastic strains development is directly controlled by means of the angle of dilation. The latter has to be properly defined to quantify the change in volume that occurs when moving from the current to the critical state. The reduction of angle of dilation with plastic shear strains can account for soil softening. The angle of dilation tends to zero as the stress path in the compression plane tends to the critical state line.

This approach corresponds to the use of a flow rule depending on the “state parameters” defined by Been and Jefferies [1] but, at the same time, simplifies the SS calibration procedure.

To obtain the six model parameters, back-figuring experimental laboratory data from simple shear tests, carried out on a specimen reconstituted at the in situ relative density, are recommended. Direct shear test results can also be used interpreting data, according to Boulon [3].

For a preliminary evaluation, it is possible to refer to the literature (Bolton [2] and Rowe [39] theories for ϕ'_p and ψ_p , respectively; Randolph et al. [36] and Stroud [43] for ϕ'_{cs} and γ^p_{cs} , respectively).

Particular attention must be paid to the choice of soil shear stiffness as its value very much depends on the stress level. An appropriate operative value of $G < G_0$ (secant stiffness) must be selected to take into account soil nonlinearity.

3.2 Shear band

To simulate the shear band, interface elements were used. Such a choice reflects the need to achieve a conveniently simple procedure for practical purposes.

The concrete–soil interface has been considered as “rough” (e.g. [21, 44]) giving rise to a shear band fully developed within the sand mass at the shaft surface. According to this premise, it has been suggested (e.g. [14, 44, 47, 51]) that soil grading mainly influences shear band thickness. Typically, t_s ranges between 5 and 20 times D_{50} , thus ranging from a few millimetres to a few centimetres for the soil under consideration. It follows that, if

continuum elements had been used for shear band simulation, very thin elements adjacent to the pile would have been considered, influencing the overall mesh (a very large number of elements would be required). The use of interface elements overcomes this limit, drastically reducing mesh conditioning and consequential numerical computation effort.

For interface elements, a constitutive law equivalent to strain softening was developed (Interface Strain Softening, ISS; [25]). This was obtained by imposing a mechanical equivalence between SS and ISS predictions when shearing is applied in simple shear mode. In detail, interface normal (k_n) and tangential (k_s) stiffness are functions of oedometric (E_{oed}) and shear moduli through shear band thickness:

$$k_n = \frac{E_{\text{oed}}}{t_s}; \quad k_s = \frac{G}{t_s} \tag{5}$$

Regarding failure conditions, the Mohr–Coulomb criterion was modified considering that interface friction angle δ' represents the resistance available along the plane of shearing. It can be easily demonstrated that, if strains in the direction of shearing can be ignored ($\delta\varepsilon_x = 0$; Fig. 5), the ratio of shear to normal stress mobilized at failure along the interface is [8]:

$$\frac{q_s}{\sigma'_{\text{hf}}} = \tan \delta' = \frac{\sin \varphi' \cdot \cos \psi}{1 - \sin \varphi' \cdot \sin \psi} \tag{6}$$

where φ' and ψ are current values, depending on plastic shear strain, γ^p . The latter is derived directly from interface displacements, δx_d :

$$\delta x_d = \delta\gamma \cdot t_s \tag{7}$$

As for SS, critical state is achieved for ISS when $x_d = x_{d,\text{cs}}^p = t_s \cdot \gamma_{\text{cs}}^p$.

When yielding occurs, coupled normal displacements, $\delta u_r = \delta\varepsilon_y \cdot t_s$, develop according to the geometrical meaning of dilatancy under conditions of plane strain:

$$\delta u_r = -\tan \psi \cdot \delta x_d^p \tag{8}$$

It follows that normal displacements generated when CS conditions are achieved depend on ψ , $x_{d,\text{cs}}^p$, t_s :

$$u_r = t_s \cdot \int_0^{x_{d,\text{cs}}^p} \tan \psi \cdot dx \tag{9}$$

Predictions of SS and ISS models were compared with experimental results obtained by Mortara [31]. In particular, CNL and CNS ($k_1 = 500$ kPa/mm) direct shear tests on fine dense sand ($I_D \approx 85$ %; $\sigma'_{v0} = 100$ kPa; $D_{50} = 0.24$ mm) were considered.

According to Boulon [3], experimental data may be interpreted by neglecting the deformation of the soil within

the two half boxes, thus concentrating all the measured effects within shear band where simple shear conditions exist. Thus, once the initial thickness t_s (in this case, a value $t_s = 20 \cdot D_{50} = 4.8$ mm has been selected) and a linear ψ reduction (Fig. 5b) are assumed, Eqs. 7 and 9 are used to find γ_{cs}^p and ψ_p , respectively. At the end of the test, when CS conditions are attained ($\psi = 0$), Eq. 6 degenerates in $\sin \varphi'_{\text{cs}} = \tan \delta'_{\text{cs}}$, hence φ'_{cs} can be derived.

Figure 6 shows the comparison between test results and numerical predictions obtained by ISS and SS. As can be seen, ISS and SS responses are superimposed and in good agreement with experimental data. As expected, the increase in q_s in the CNS test, with respect to the CNL test, is remarkable and consistent with the increase in normal stress, σ'_n .

3.3 Boundary value problem

Numerical axisymmetric analyses of single piles, embedded in sandy soils and axially loaded (in compression), were carried out by means of the commercial finite difference code FLAC 2D.

Piles were considered “wished-in-place”, without altering the pre-existing state of stress in the soil mass around the pile, thus ideally supposing that concreting can reinstate the effective horizontal stress existing before drilling [13]. It is believed that, in the absence of specific information, such an assumption is considered reasonable. However, the study of construction effects on shaft capacity is beyond the scope of this research.

While the SS model for soil was already available in the library code, ISS for interfaces was developed by writing an appropriate FISH routine.

The pile was modelled as continuum elements, with an isotropic linear elastic constitutive model.

Figure 7 reports the finite difference mesh used for the analyses: lateral boundaries of the mesh were restrained horizontally, while the base at a depth $H = 2 \cdot L$ was prevented from moving either vertically or horizontally. Model width and mesh density were established by sensitivity analyses to guarantee the solution accuracy [25]. Particular attention was paid to define the mesh close to the pile to prevent errors due to stress concentration.

Axial pile load tests were simulated according to the displacement control technique up to the full mobilization of the shaft friction: a fictitious vertical velocity of 10^{-7} m/step was applied at the pile head, thus low enough to make inertial effects negligible and to ensure solution accuracy.

Simulations were performed under small strain conditions.

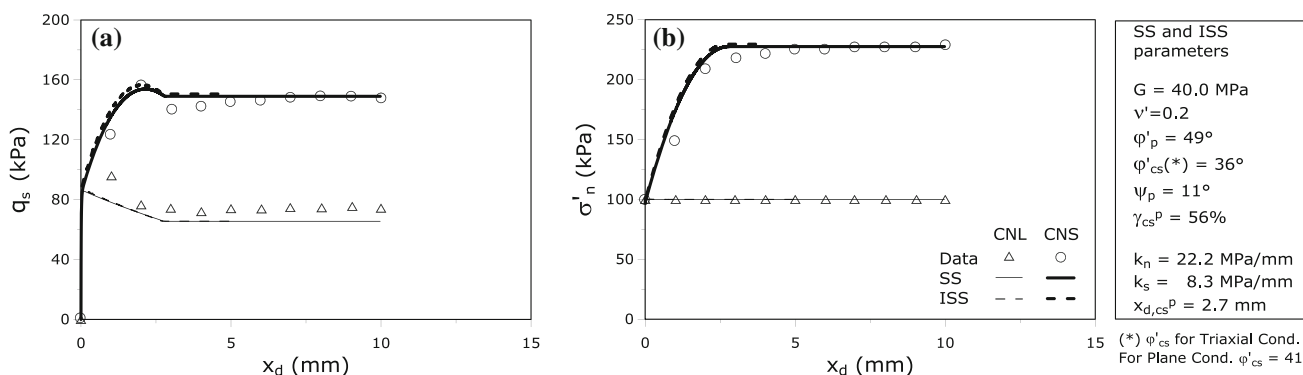


Fig. 6 Comparison between experimental results [31] and predictions of SS and ISS models for CNL and CNS shear tests

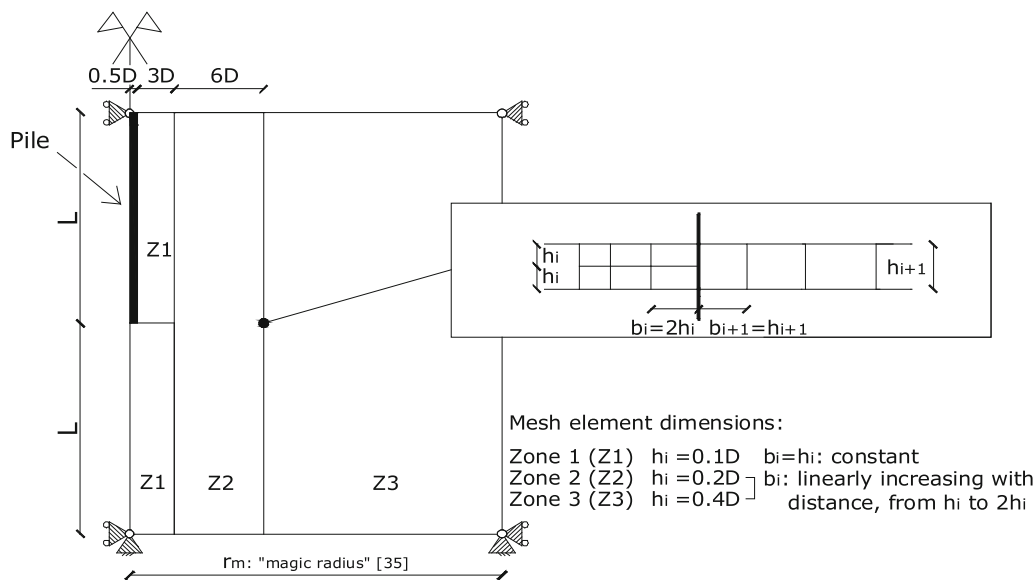


Fig. 7 Geometry, mesh and boundary kinematic constrains of problem under investigation

4 Numerical results

To investigate the role played by single factors influencing the pile shaft capacity (relative density, stress history, critical state friction angle and shear band thickness), a broad parametric study was conducted.

Table 2 summarizes data for the whole spectrum of analyses: a suite of 96 different combinations was performed. Pile diameter was set equal to $D = 1$ m, while two lengths were considered ($L = 15$ m, 40 m). Typical concrete properties were selected: unit weight, $\gamma_{conc} = 25$ kN/m³, Young’s modulus, $E_{conc} = 30$ GPa; Poisson’s ratio, $\nu'_{conc} = 0.25$.

Soil unit weight was set equal to $\gamma_s = 17$ kN/m³; dry or saturated soil conditions were considered. Critical state angle and relative density fall within typical ranges: $\phi'_{cs} = 32^\circ$ – 38° [36]; $I_D = 30$ – 50 – 70 % and kept constant along the depth for each case. Normally consolidated (NC) and over-consolidated (OC) soils were considered.

Regarding the latter, the OCR profile is shown in Fig. 8, with the corresponding K_0 profiles (Eq. 2, with $\phi' = \phi'_{cs}$ as suggested by Mesri and Hayat [29] and $K_0 \leq 1$ as suggested by Jamiolkowski et al. [16]).

Angles of friction and dilation at peak were evaluated according to Bolton [2] and Rowe [39], respectively, thus continuously varying with depth due to p' changes (being I_D constant for each case). A linear reduction for ϕ'_p and ψ_p was supposed (Fig. 5b). According to several experimental data (e.g. [31, 43]), γ_{cs}^p typically falls within the range 40–80 %; a value $\gamma_{cs}^p = 60$ % was assumed.

For all the analyses, Poisson’s ratio was kept constant and equal to 0.2 (typical for sandy soils, e.g. [18]). Three different G_0 profiles, linearly varying with depth, were assumed for different I_D values (Table 2). To take into account soil nonlinearity, all the analyses presented were carried out with $G/G_0 = 0.5$. Clearly such a choice does not affect the results of the parametric analyses from a qualitative point of view. This choice is crucial when the

Table 2 Fundamental data of parametric analyses

Parameter	Value	Description
L	15 m	Long pile
	40 m	Short pile
φ'_{cs}	32°	$\varphi'_{cs} = 32^\circ$
	38°	$\varphi'_{cs} = 38^\circ$
I_D	70 %	Dense sand
	50 %	Medium dense sand
	30 %	Loose sand
K_0	0.47	NC_ $\varphi'_{cs} = 32^\circ$
	0.38	NC_ $\varphi'_{cs} = 38^\circ$
	1 ^a	OC (max value)
t_s	4 mm	Fine sand
	40 mm	Coarse sand
G_0 (MPa)	30 + 2·z (m)	$I_D = 30\%$
	46 + 2·z (m)	$I_D = 50\%$
	65 + 2·z (m)	$I_D = 70\%$

^a In OC soils, K_0 reduces along depth following OCR reduction; in any case $K_0 \leq 1$ [16]

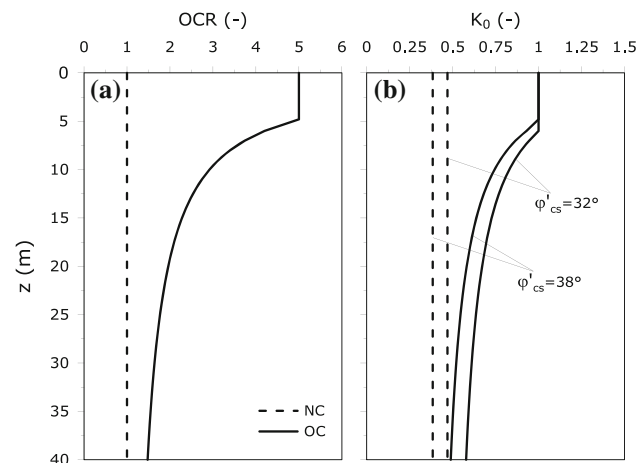


Fig. 8 Parametric analyses: **a** OCR and **b** K_0 profile for NC and OC models

analyses aim to reproduce experimental data by a simple model, such as SS, as discussed below.

Lastly, two shear band thicknesses were simulated: $t_s = 4\text{--}40$ mm (corresponding to $D_{50} = 0.2\text{--}2$ mm if $t_s = 20 \cdot D_{50}$ is assumed).

4.1 Typical results of a single pile

Results of Analysis N. 8, whose input parameters are reported in Fig. 9, are outlined in Fig. 10.

In detail, in Fig. 10a, b the evolution of q_s , σ'_h and u_r versus local pile displacements inside the shear band are

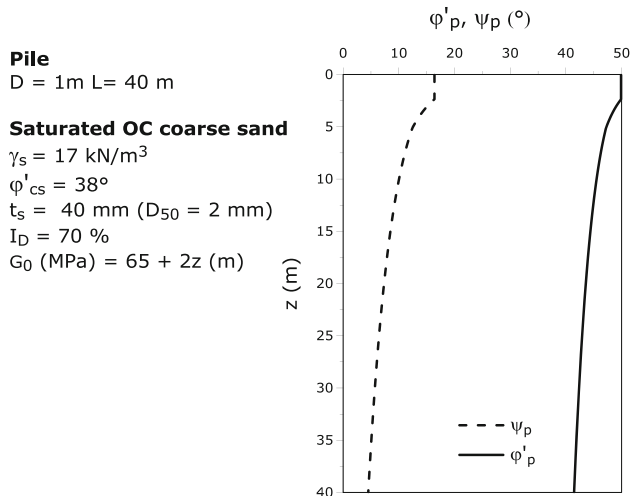


Fig. 9 Analysis N. 8: pile geometry and geotechnical model

represented for different depths. During loading, the effects of partially restrained radial displacements (u_r) are clear, since horizontal stresses significantly arise. Due to the increase in confinement, dilatant effects decrease with depth. Moreover, at the top of the pile, volumetric plastic strains develop in soil surrounding shear band, thus contributing to σ'_h increase. Stress evolution in the interface layer at different depths during loading is shown in Fig. 10d. Despite softening, q_s increases up to CS condition, according to that experimentally observed by Lehane et al. [19] (Fig. 3).

In Fig. 10c, β values at the end of the loading are presented. As expected, a typical decreasing profile with depth is obtained, very similar to that systematically deduced from experimental tests on instrumented piles.

Figure 10e also reports the load–settlement curves at pile head, Q , at pile shaft, Q_s , and at pile base, Q_b . All quantities are dimensionless, since loads refer to the ultimate value of the total capacity, Q_u , and displacements, w , to the pile diameter, D . As can be seen, Q_s is fully mobilized when pile head displacement approaches the value $w = 4\% \cdot D$; at this value, Q_b is still far from its ultimate value.

4.2 Parametric analyses

Figure 11 shows Q_s and β profiles for different combination of I_D , t_s , OCR and φ'_{cs} values. To be noted is the major role played by relative density, which is in turn enhanced by interface thickness and hence by soil grading (Fig. 11a). In finer soils ($t_s = 4$ mm), shaft resistance increases about 1.5 times ($Q_{s,70\%}/Q_{s,30\%} \approx 1.5$) only by changing relative density from 30 to 70 %. This ratio approaches 2.5 if coarser soils are considered ($t_s = 40$ mm). These effects are a direct outcome of the proportionality between u_r and t_s .

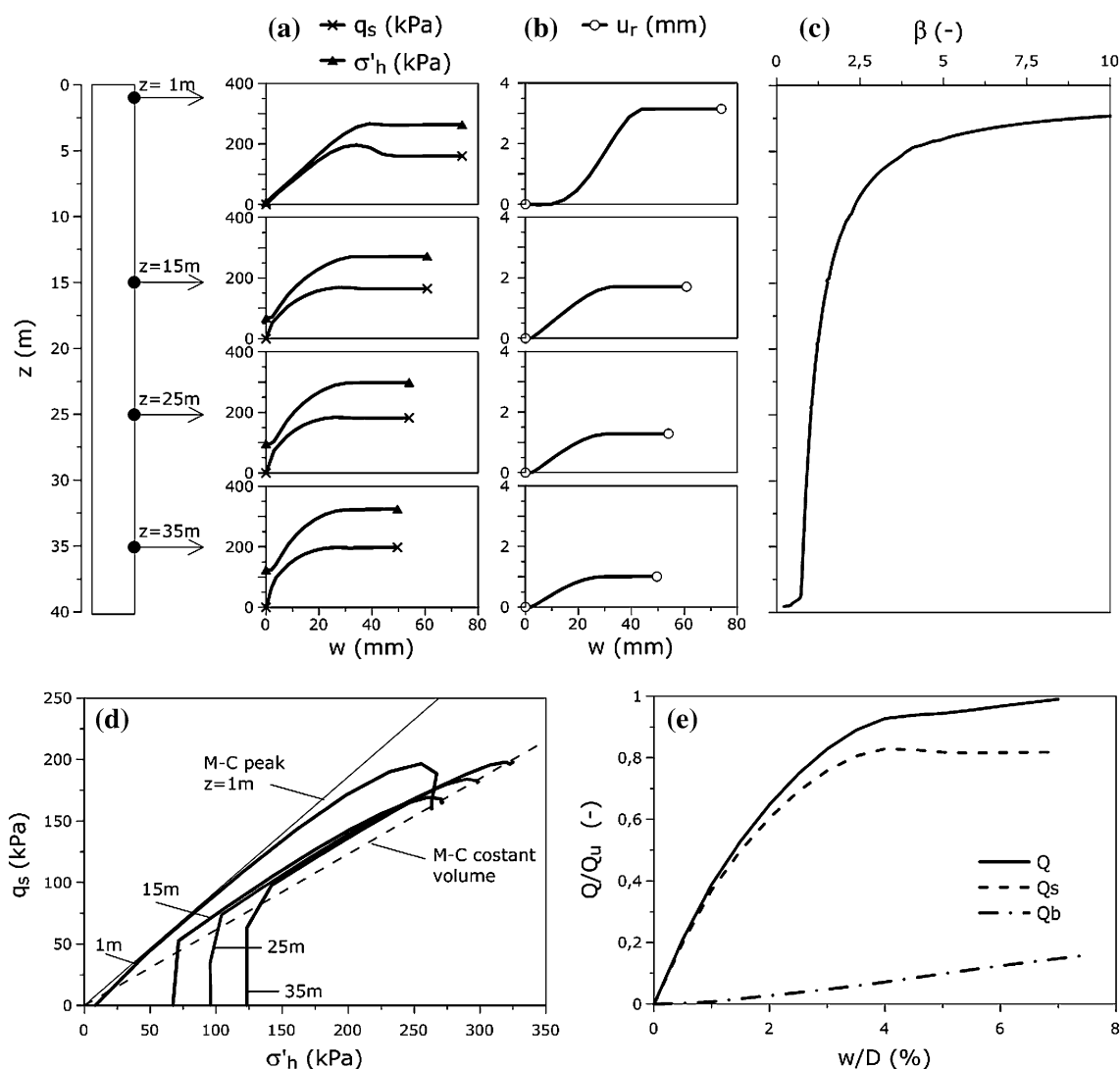


Fig. 10 Analysis N. 8, load test results: **a** stresses, **b** radial displacements evolution and **d** stress paths in the shear band along depth; **c** β profile; **e** load–displacement curves

Increments of shaft capacity less than 1.5 are ascribable to pre-existing horizontal stress profile (σ'_{h0}), directly linked to the stress history of the model (OCR; Fig. 11b). In OC soils, the higher skin friction is due to larger values of the earth coefficient at rest K_0 , irrespective of shear band thickness. CS friction angle plays a minor role, inducing small variations of Q_s (Fig. 11c).

Focussing attention on the resistance increase induced by the stress changes during loading along the shaft, the results from all 96 analyses are also represented in terms of β/β_0 versus normalized effective mean stress p'/p_{atm} (Fig. 12; $\beta_0 = K_0 \cdot \tan \delta'$ represents the reference value of the shaft resistance that would be mobilized if horizontal stress did not change). It is evident that, for cases where I_D and t_s are equal, all the curves are practically superimposed, thus producing a very narrow band. It is also evident that, for the

same soil state (relative density and mean stresses), fine sands cannot develop large values of q_s as a consequence of a very thin shear band (small t_s) giving rise to very small u_r (Eq. 9); the opposite holds for coarse sands.

To boost the effects of shear band thickness, further 9 analyses were performed (NC, $\varphi'_{cs} = 38^\circ$, saturated, $L = 40$ m, $I_D = 30$ – 50 – 70 %) with additional values for t_s (0.2–2–20 mm).

The main results obtained for loose and dense soils ($I_D = 30$ – 70 %) are shown in Fig. 13. The horizontal stresses at the end of the load are quantified by K/K_0 ratio “measured” at the interface along the pile shaft, for different confinement values ($p'/p_{atm} = 0.25$ – 1.5). Since the solution does not depend on the absolute values for t_s and D , but on their ratio (e.g. [22, 25]), results are represented in terms of t_s/D .

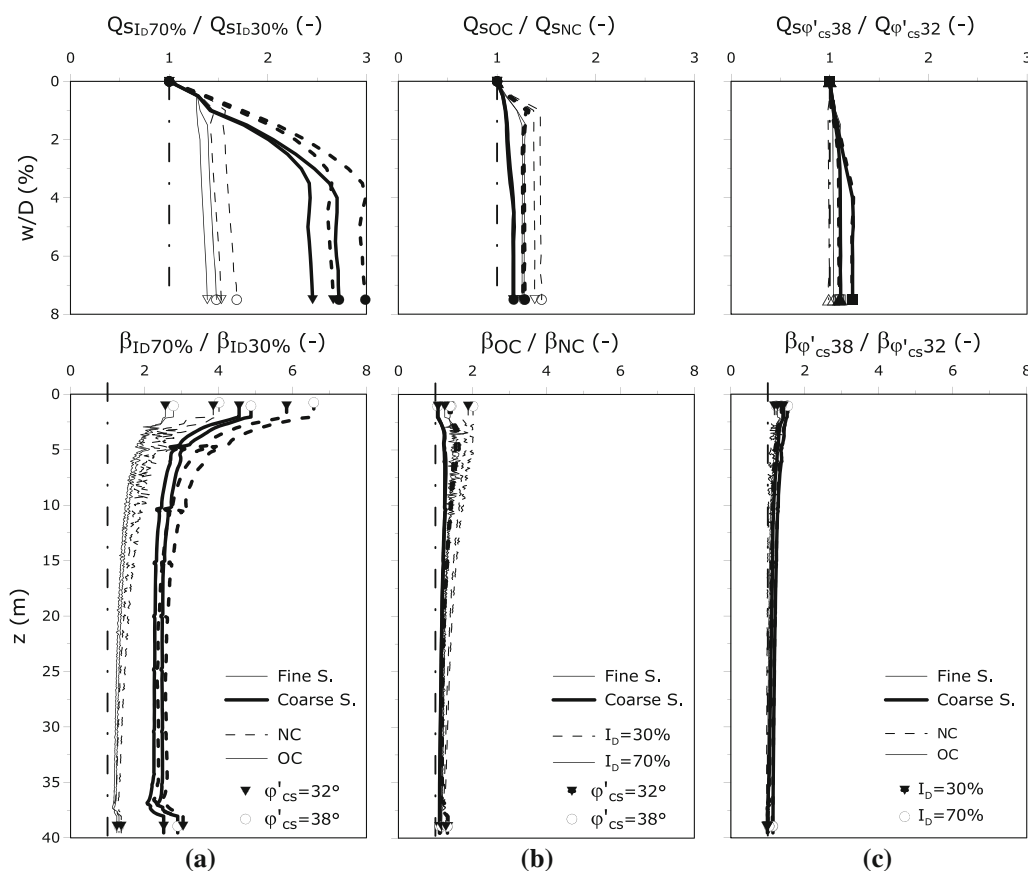


Fig. 11 Parametric analyses, wet models: Q_s and β increments by changing t_s and I_D , (b) OCR, (c) ϕ'_{cs}

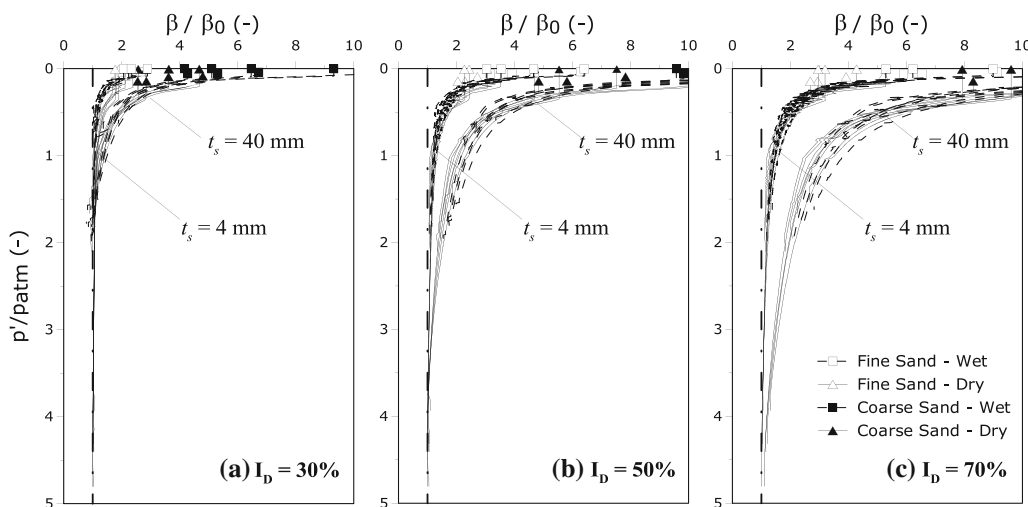


Fig. 12 Parametric analyses: β/β_0 profiles versus p'/p_{atm} by changing I_D , OCR, ϕ'_{cs} and t_s in wet and dry models

The ratio K/K_0 decreases as shear band thickness reduces. The thinner the interface layer is, the smaller u_r is, irrespective of soil dilation potential. When $t_s/D \rightarrow 0$, interface layer expansion is very small ($\sigma'_{hf} \rightarrow \sigma'_{h0}$ and $K/K_0 \rightarrow 1$): values of K/K_0 slightly larger than unity reflect the pile radial expansion (Poisson's effect). Similar results

have been published by Loukidis and Salgado [22]. They suggested values $K/K_0 > 2$ when $t_s/D \rightarrow 0$, higher than those reported in this paper, despite the fact that in their model the pile is rigid, and therefore, Poisson's effect is absent. Such an aspect appears to be controversial and requires further investigation.

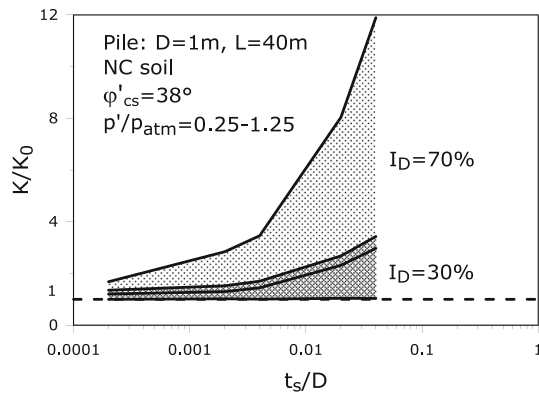


Fig. 13 Parametric analyses: K/K_0 versus t_s/D by changing I_D and p'

5 Case history: experimental site at the eastern area of Naples

Several pile load tests have been performed for the design of the foundation of the Naples Law Courts' Tower [5, 46], in the eastern area of the city. The foundation consists of a reinforced concrete slab resting on 241 bored piles with a length of 42 m and diameters ranging between 1.5 and 2.2 m.

The subsoil of the whole area has been thoroughly investigated by a number of authors (a summary is given by Mandolini [23]) and is well known with regard to its general features. Starting from the ground surface and moving downwards, the following soils are found:

- top soil ($\approx 0-10$ m);
- stratified sands ($\approx 10-25$ m);
- pozzolana, cohesion-less ($\approx 25-35$ m) and slightly cemented (>35 m).

Table 3 Properties for Neapolitan pyroclastic soils

Layer	z (m)	γ (kN/m ³)	ϕ'_{cs} (°)	t_s min (mm)	t_s max (mm)
Top soil (sand, gravel)	0	15	32	40	80
	10.4				
Sand	10.4	17	35	10	20
	24.8				
Cohesion-less pozzolana	24.8	17	36	1.2	4
	35.2				
Slightly cemented pozzolana	35.2	17	36	4	20
	42				

The groundwater table lies at an average depth of 3 m below ground surface.

The overall set of input soil parameters employed in the numerical analyses is reported in Fig. 14 (dotted line) and Table 3.

A representative result of CPT is reported in Fig. 14, together with the horizontal stress profile and the main geotechnical parameters as derived according to Chen and Kulhawy [6] for σ'_h , Schanz and Vermeer [40] and Mayne [27] for ϕ'_p in plane condition, Rowe [39] for ψ_p , Schnaid et al. [41] for G_0 ; a secant value $G = G_0/2$ was then used. The critical state angle, ϕ'_{cs} , was fixed according to laboratory tests (Table 3); ϕ'_p and ψ_p were assumed to reduce linearly (Fig. 5b; $\gamma^p_{cs} = 60\%$).

A variable grain size for each soil type along depth emerged from laboratory tests, as well as from the literature (e.g. [32]). Consequently, two different sets of values were considered for the shear band thickness ($t_s = 20 \cdot D_{50}$) in order to simulate extreme conditions (Table 3).

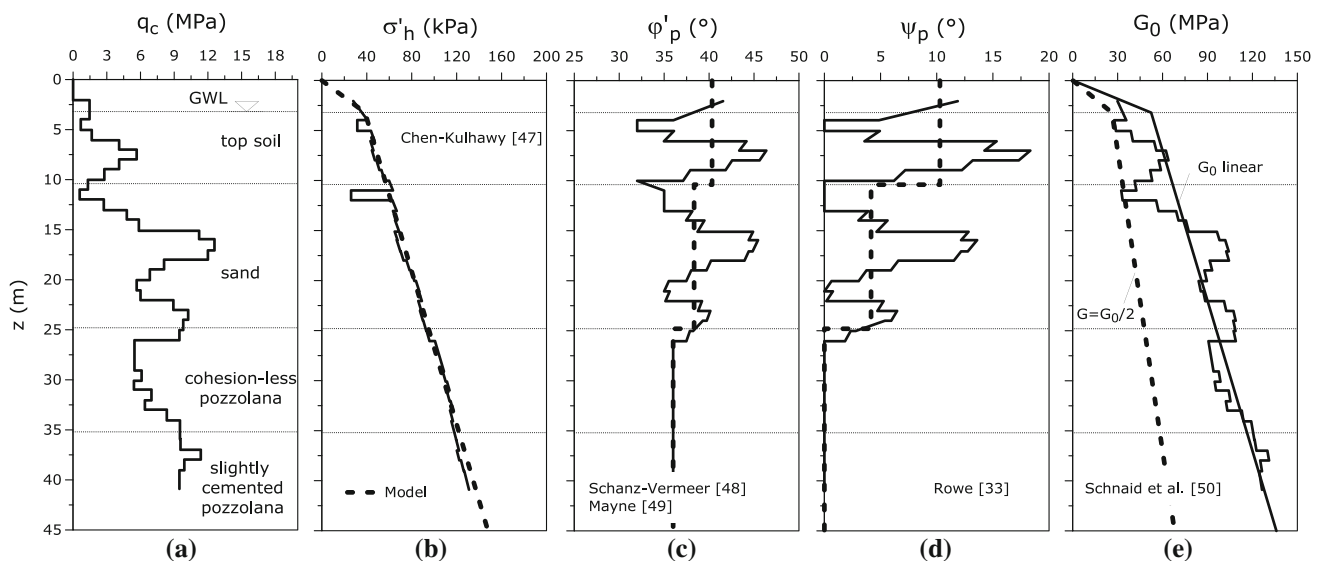


Fig. 14 Geotechnical profile: (a) q_c , (b) σ'_{h0} , (c) ϕ'_p , (d) ψ_p and (e) G_0

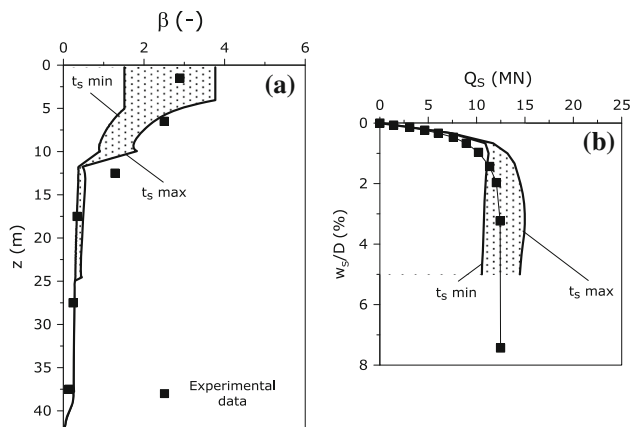


Fig. 15 Comparison between predicted and measured pile response: **a** β profile and **b** shaft load–displacement curve

Before the installation of production piles, four trial piles were loaded to failure. These piles, 42 m length and 1.5–2 m in diameter, were instrumented along the shaft and were loaded up to maximum load (ranging between 15.0 and 26.5 MN). A detailed description of each load test can be found in Viggiani and Vinale [46] and Caputo et al. [5].

In the following, the results of only one pile load test are presented ($D = 1.5$ m; $L = 42$ m): the measured and predicted β profiles are reported in Fig. 15a; the shaft load–settlement curve is reported in Fig. 15b.

The agreement between experimental measurements and theoretical solutions is rather good. As expected, if the angle of dilation is null (cohesion-less and slightly cemented pozzolana), the change in horizontal stress during loading is negligible and shear band thickness does not affect β values. The more rigid pile response to loading, as predicted by numerical analyses, derives from the assumption that soil behaves as linear elastic until the peak strength is attained (SS and ISS models).

6 Concluding remarks

The estimation of the shaft capacity of cast in situ bored piles in sands is typically conducted using empirical methods based on the measured response of loading tests. They are simple to apply, but are too simplistic. They fail to adequately take into account the fundamental aspects of the behaviour of sandy soil and the complex phenomena occurring in the thin cylinder of soil surrounding the pile (shear band).

Based on an understanding of the physical and mechanical phenomena that develop at pile–soil interface during loading, a numerical approach to estimate shaft friction of bored piles in sands is presented.

The localization of plastic shear strains in the shear band is explicitly modelled using interface elements. The

constitutive law selected for both soil and interface is quite simple, and it is able to reproduce the main aspects of the mechanical behaviour of sandy soils.

The proposed approach takes into account the increase of shaft friction associated with the increase of horizontal stresses during axial loading. This can be mainly ascribed to soil dilatancy in the shear band, partially restrained by confining soil, and to pile Poisson's effect. Its use is relatively simple as it is based on a small number of parameters, most of which are available from routine geotechnical investigations (soil unit weight, soil grading, geostatic stresses, strength and stiffness parameters and groundwater condition). Additional information can be derived from simple or direct shear tests results on specimens reconstituted at the in situ relative densities.

The broad parametric analyses performed aimed to detect which factors (t_s/D , I_D , p'/p_{atm}) most affect the piles' shaft capacity. The tendency of the soil to dilate depends on the soil state (I_D , p'/p_{atm}); however, its effect on shaft friction strongly depends on t_s/D . Given the same soil state, piles embedded in coarse sandy soils would mobilize larger shaft resistance than in finer sand, due to the very different volumetric expansion in the shear band that occurs for each.

Future research efforts should be directed towards defining experimental laboratory procedures and interpretation criteria to quantify the total expansion of the shear band due to dilatancy. Further research is called for to define operative values of soil shear stiffness.

It is the authors' opinion that the proposed method would be of particular use in those instances where model piles (reduced length and/or diameter) are installed in the same soil (D_{50}) and then tested. Once the results from the model pile are back-figured, it would be relatively simple to extend the results to the full-scale pile.

It goes without saying that the availability of a large number of well-documented, full-scale load tests on instrumented bored piles, such as those reported here, could help improve the proposed procedure, making it applicable in practice. The back-analysis of experimental data, together with further research activities, would also lead to a better understanding on the effect of pile installation.

References

1. Been K, Jefferies MG (1985) A state parameter for sands. *Géotechnique* 35(2):99–112
2. Bolton MD (1986) The strength and dilatancy of sands. *Géotechnique* 36(1):65–78
3. Boulon M (1988) Numerical and physical modelling of piles behaviour under monotonous and cyclic loading. In: *International symposium SOWAS'88, Delft*, pp 285–293

4. Boulon M, Foray P (1986) Physical and numerical simulation of lateral shaft friction along offshore piles in sand. In: Proceedings of the 3rd international conference on numerical methods in offshore piling, Nantes, pp 127–147
5. Caputo V, Mandolini A, Viggiani C (1993) Large diameters bored piles in pyroclastic soils. In: Van Impe (ed) Deep foundations on bored and auger piles. Milpress, Rotterdam, pp 227–232
6. Chen YJ, Kulhawy FH (1994) Case history evaluation of the behaviour of drilled shafts under axial and lateral loading. Final report, Project 1493-04, EPRI TR-104601, Geotechnical Group, Cornell University, Ithaca
7. Chen YJ, Kulhawy FH (2002) Evaluation of drained axial capacity for drilled shafts. In: O'Neill MW, Townsend FC (eds) Geotechnical special publication no. 116, deep foundations 2002, ASCE, Reston, VA, pp 1200–1214
8. Davis EH (1968) Theories of plasticity and the failure of soil masses. Soil Mechanics, Selected Topics. Ed. I. K. Lee, Butterworth
9. De Nicola A, Randolph MF (1993) Tensile and compressive shaft capacity of piles in sand. J Geotech Eng 119(12):1952–1973
10. Falconio G, Mandolini A (2003) Influence of residual stresses for non displacement cast in situ piles. In: Van Impe (ed) Deep foundations on bored and auger piles. Milpress, Rotterdam, pp 145–152
11. FHWA (2010) Drilled shafts: construction procedures and LRFD design methods. U.S. Department of Transportation Federal Highway Administration, NHI Course N. 132014
12. Fioravante V (2002) On the shaft modelling of non-displacement piles in sand. Soils Found 42(2):23–33
13. Fleming WGK, Weltman AJ, Randolph MF, Elson WK (2009) Piling engineering. Taylor and Francis, London
14. Frost JD, Hebel GL, Evans TM, DeJong JT (2004) Interface behaviour of granular soils. In: Engineering construction and operations in challenging environments earth and space 2004. Proceedings of the 9th biennial ASCE aerospace division international conference. League City, Houston, TX
15. Jaky J (1944) The coefficient of heart pressure at rest. Journal of the Society of Hungarian Architects and Engineers, Budapest, pp 355–358
16. Jamiolkowski M, Ghionna V, Lancellotta R, Pasqualini E (1988). New correlations of penetration tests for design practice. In: Proceedings of the international symposium of penetration testing, IS-OPT-1, Orlando, vol 1. AA Balkema, The Netherlands, pp 263–296
17. Jardine RJ, Chow FC, Overy R, Standing J (2005) ICP design methods for driven piles in sands and clays. Thomas Telford, London
18. Lehane B, Cosgrove E (2000) Applying triaxial compression stiffness data to settlement prediction of shallow foundations. Geotech Eng 142:191–200
19. Lehane BM, Jardine RJ, Bond AJ, Frank R (1993) Mechanisms of shaft friction in sand from instrumented pile tests. J Geotech Eng 119(1):19–35
20. Lehane BM, Gaudin C, Schneider JA (2005) Scale effects on tension capacity for rough piles buried in dense sand. Géotechnique 55(10):709–719
21. Lings ML, Dietz MS (2005) The peak strength of sand-steel interfaces and the role of dilation. Soils Found 45(6):1–14
22. Loukidis D, Salgado R (2008) Analysis of the shaft resistance of non-displacement piles in sand. Géotechnique 58(4):283–296
23. Mandolini A (1994). Cedimenti di fondazioni su pali. Ph.D. Thesis. Consorzio tra le Università di Roma La Sapienza, Federico II di Napoli, Seconda Università di Napoli
24. Manzari M, Dafalias Y (1997) A critical state two-surface plasticity model for sands. Géotechnique 47(2):255–272
25. Mascarucci Y (2012) Un nuovo approccio per la valutazione della resistenza laterale in terreni sabbiosi. Ph.D. Thesis. Sapienza University of Roma
26. Mascarucci Y, Mandolini A, Miliziano S (2013) Effects of residual stresses on shaft friction of bored cast in situ piles in sand. J Geo-eng Sci 1(1):37–51
27. Mayne PW (2006) Undisturbed sand strength from seismic cone tests. The 2nd James K. Mitchell Lecture. J Geomech Geoen 1(4):239–258
28. Mayne PW, Kulhawy FH (1982) K_0 -OCR relationships in soil. J Geotech Eng Div ASCE 108(6):851–872
29. Mesri G, Hayat TM (1993) The coefficient of heart pressure at rest. Can Geotech J 30:647–666
30. Meyerhof GG (1976) Bearing capacity and settlement of pile foundations. J Geotech Eng Div ASCE 102(GT3):197–228
31. Mortara G (2001) An elastoplastic model for sand-structure interface behaviour under monotonic and cyclic loading. Ph.D. Thesis. Technical University of Torino
32. Pellegrino A (1967) Proprietà fisico meccaniche dei terreni vulcanici nel Napoletano. AGI VIII Convegno di geotecnica, Cagliari, vol 3, pp 113–145
33. Peng SY, Ng CWW, Zheng G (2013) The dilatant behaviour of sand-pile interface subjected to loading and stress relief. Acta Geotechnica. doi:10.1007/s11440-013-0216-9
34. Randolph M, Gourvenec S (2011) Offshore geotechnical engineering. Taylor & Francis, London
35. Randolph MF, Wroth CP (1978) Analysis of deformation of vertically loaded piles. J Geotech Eng Div ASCE 104(12):1465–1488
36. Randolph MF, Jamiolkowski MB, Zdravkovic L (2004) Advances in geotechnical engineering. In: The Skempton conference, vol 1, pp 207–240
37. Reese LC, O'Neill MW (1988) Drilled shafts: construction and design. FHWA, Publication no. HI-88-42
38. Rollins KM, Clayton RJ, Mikesell RC, Blaise BC (2005) Drilled shaft side friction in gravelly soils. J Geotech Geoenv Eng ASCE 131:987–1003
39. Rowe PW (1962) The stress-dilatancy relation for static equilibrium of an assembly of particles in contact. Proc R Soc London Ser A 269(1339):500–527
40. Schanz T, Vermeer PA (1996) Angles of friction and dilatancy of sand. Géotechnique 46(1):145–151
41. Schnaid F, Lehane BN, Fahey M (2004) In situ test Characterization of unusual geomaterials. In: Proceedings of the 2nd international conference on site characterization, vol 1. Milpress, Porto, pp 49–74
42. Schneider JA (1997) Analysis of piezocone data for displacement pile design. PhD Thesis, Western Australia University
43. Stroud MA (1971) The behaviour of sand at low stress levels in the simple shear apparatus. PhD Thesis, University of Cambridge
44. Uesugi M, Kishida H (1986) Influential factors of friction between steel and dry sand. Soils Found 26(2):29–42
45. Viana da Fonseca A, Santos JA (2008) Behaviour of CFA, driven and bored piles in residual soil. In: International prediction event—experimental site—ISC'2. FEUP/IST Portugal
46. Viggiani C, Vinale F (1983) Comportamento di pali trivellati di grande diametro in terreni piroclastici. Riv Ital Geotecnica 23(2):59–84
47. Viggiani G, Kuntz M, Desrues J (2001) An experimental investigation of the relationship between grain size distribution and shear banding in granular materials. In: Vermeer PD et al (eds) Continuous and discontinuous modelling of cohesive-frictional materials, vol 568. Springer, Berlin, pp 111–127
48. Viggiani C, Mandolini A, Russo G (2012) Piles and pile foundations. Ed. Spon Press, Taylor & Francis, London

49. Wernick E (1978) Skin friction of cylindrical anchors in non-cohesive soils. In: Symposium on soil reinforcing and stabilising techniques, pp 201–219
50. Wood DM (2004) Geotechnical modelling. Ed. Spon Press, Taylor & Francis, London
51. Yang ZX, Jardine RJ, Zhu BT, Foray P, Tsuha CHC (2010) Sand grain crushing and interface shearing during displacement pile installation in sand. *Géotechnique* 60(6):469–482